NANO LETTERS

2007
Vol. 7, No. 1
93−100

Optical and Magnetic Resonance Imaging of Cell Death and Platelet Activation Using Annexin A5-Functionalized Quantum Dots

Lenneke Prinzen,*,† Robbert-Jan J. H. M. Miserus,‡ Anouk Dirksen,§ Tilman M. Hackeng,§ Niko Deckers,§ Nicole J. Bitsch,|| Remco T.A. Megens,† Kim Douma,† Johan W. Heemskerk,§ M. Eline Kooi,‡ Peter M. Frederik,⊥ Dick W. Slaaf,†,# Marc A. M. J. van Zandvoort,† and Chris P. M. Reutelingsperger§

Department of Biophysics, University of Maastricht, Department of Radiology, University Hospital Maastricht (azM), Department of Biochemistry, University of Maastricht, Department of Cardiology, University of Maastricht, and Department of Pathology, Electron Microscopy Unit, University of Maastricht, Maastricht, The Netherlands, and Department of Biomedical Engineering, Technische Universiteit Eindhoven, Eindhoven, The Netherlands

Received September 21, 2006; Revised Manuscript Received November 30, 2006

ABSTRACT

A quantum-dot-based nanoparticle is presented, allowing visualization of cell death and activated platelets with fluorescence imaging and MRI. The particle exhibits intense fluorescence and a large MR relaxivity (r_1) of 3000−4500 mM^{-1} s^{-1} per nanoparticle due to a newly designed construct increasing the gadolinium-DTPA load. The nanoparticle is suitable for both anatomic and subcellular imaging of structures in the vessel wall and is a promising bimodal contrast agent for future in vivo imaging studies.

Contrast-enhancing nanoparticles are essential in the field of molecular imaging. Molecular imaging focuses on early detection of various diseases and supports personalized therapy. While conventional imaging modalities such as computer tomography and magnetic resonance imaging (MRI) allow visualization of anatomical and (patho)physiological consequences of the disease, molecular imaging is based on the molecular and cellular fingerprints of the disease, requiring disease-specific molecular targets as well as target-specific nanoparticles. Furthermore, these nanoparticles should allow visualization in vivo with sufficient perceptibility.

Programmed cell death (PCD) is a process of organized cell suicide and occurs in various forms, of which apoptosis is the best known.[1] PCD plays important roles in physiology as well as pathology of multicellular organisms. During homeostasis, a balance exists between cell proliferation and cell death. This equilibrium is disturbed under certain pathological conditions. Acute myocardial infarctions,[2] heart failure,[3] or unstable atherosclerotic plaques[4,5] show increased PCD, whereas in cancer, this balance shifts toward cell proliferation.[6] Anticancer therapies are being developed in which PCD is induced in cancer cells to reverse tumor growth.[7−9] Because of the role of PCD in numerous diseases, imaging of this process would be of great value to diagnosis and guidance of therapy.

One of the most explored molecular imaging targets of PCD is phosphatidylserine (PS). This aminophospholipid is translocated from the inner to the outer leaflet of the cellular membrane in dying cells, triggering phagocytosis.[10] Cell surface exposure of PS occurs during most types of cell death,[8] but is not limited to dying cells. For example, blood platelets expose PS in an advanced stage of activation,[11,12] providing a physiological surface for blood coagulation processes. Hence, molecular imaging of PS can also be of value to diagnosis and management of thrombotic diseases.

* Corresponding author. E-mail: L.Prinzen@bf.unimaas.nl. Address: University of Maastricht, Department of Biophysics, P.O. Box 616, 6200 MD Maastricht, The Netherlands. Telephone: +31 43 3881661. Fax: +31 43 3670916.

† Department of Biophysics, University of Maastricht.

‡ Department of Radiology, University Hospital Maastricht (azM).

§ Department of Biochemistry, University of Maastricht.

|| Department of Cardiology, University of Maastricht.

⊥ Department of Pathology, Electron Microscopy Unit, University of Maastricht.

Department of Biomedical Engineering, Technische Universiteit Eindhoven.

10.1021/nl062226r CCC: $37.00
Published on Web 12/14/2006

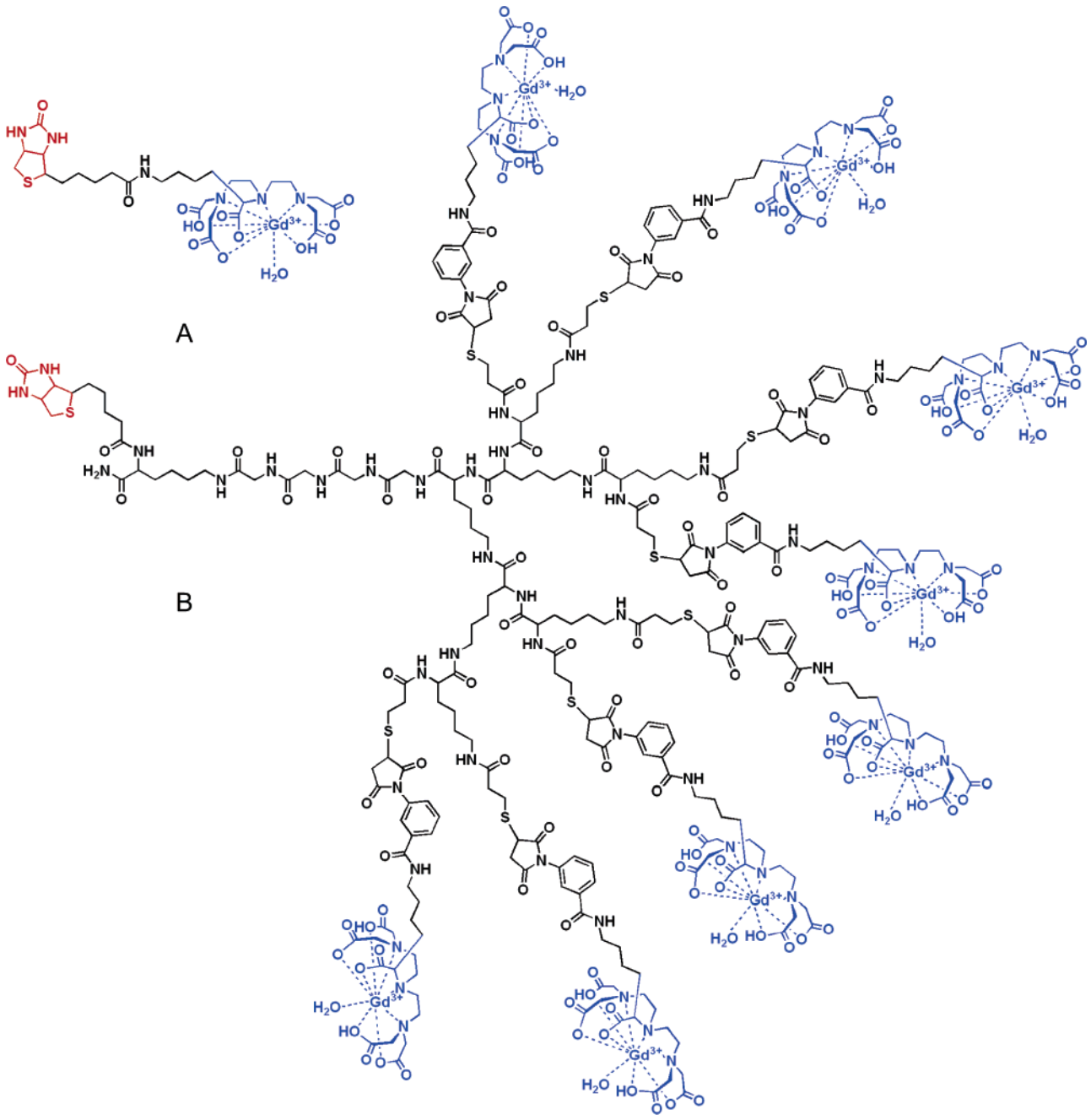

Figure 1. Molecular structure of the biotinylated Gd-DTPA (A) and biotinylated Gd-wedge (B) structures with biotin (red) and Gd-DTPA (blue).

Annexin A5 (AnxA5) is a well-explored molecular imaging probe to visualize cell surface exposure of PS.[13] AnxA5 binds to PS with a Kd in the nM range in the presence of Ca^{2+} ions.[14] It can be coupled to a variety of reporter compounds, making it suitable to use in combination with various imaging modalities including optical,[15,16] nuclear,[17,18] and magnetic resonance imaging (MRI).[19,20] In vivo studies in animals and patients demonstrated that AnxA5 can be used to noninvasively detect the vulnerability of atherosclerotic plaques,[21,22] size, and location of the infarct region in acute myocardial infarctions,[2] the extent of liver apoptosis,[23,24] and the localization of mural thrombi in abdominal aortic aneurisms.[25] In addition, imaging cell death with AnxA5 allows early assessment of the efficacy of anticancer therapy.[9] These studies utilized radioactively labeled AnxA5 in combination with single photon emission computed tomography (SPECT) or positron emission tomography (PET). SPECT and PET imaging do not yield anatomical information and have a relatively poor resolution: 8−14 mm for SPECT and 4−7 mm for PET.[17,26] These limitations can be overcome by MRI using targeted contrast agents. MRI has a better resolution (±300 μm)[26] and provides anatomical information, enabling a more accurate localization and characterization of the target site. However, sensitivity of this imaging modality for contrast agents is still relatively low.

In this paper a new, AnxA5-functionalized and bimodal nanoparticle is presented that is suitable for MRI and

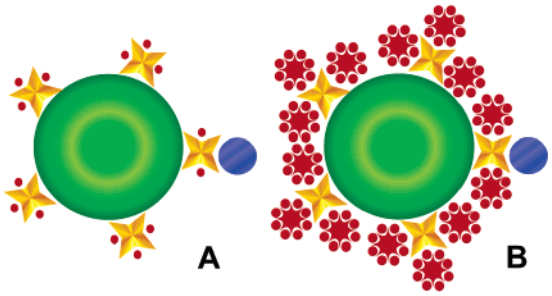

Figure 2. Schematic representation of the two nanoparticles. QDs contain approximately 1 AnxA5 and 10 streptavidin molecules. (A) Nanoparticle with single biotinylated Gd-DTPA (AnxA5-QD-Gd). (B) Nanoparticle with the biotinylated Gd-wedge, containing eight Gd-DTPA complexes each (AnxA5-QD-Gd-wedge). Green: QD; yellow: streptavidin; red dot: Gd-DTPA; red star: lysine-wedge; blue: AnxA5.

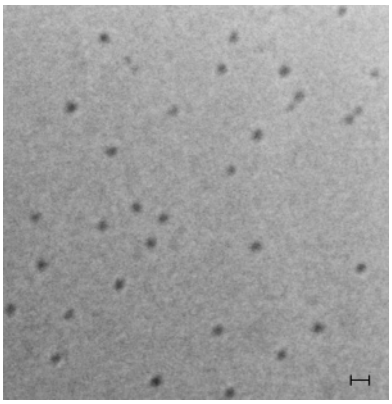

Figure 3. Cryo transmission electron microscopy image of AnxA5-QD525-Gd. Bar = 10 nm.

fluorescence imaging, allowing analysis at the anatomical as well as subcellular level. The nanoparticle is based on a quantum dot (QD), which is intensely fluorescent. The emission wavelength of QDs can be varied by altering the size of the semiconductor crystal core. Emission spectra of QDs are very narrow: emission peak width is about 20 nm at half-maximum. Furthermore, QDs with different emission wavelengths have the same excitation wavelength. These properties allow multicolor analysis of samples in a single procedure.[27] A recent publication by Le Gac et al.[28] showed that QDs (Quantum Dot Corporation, now Invitrogen) resist photobleaching and allow therefore imaging of fast, cellular processes over a longer period of time as compared to organic fluorescent dyes.

Long term in vivo effects of QDs are unknown so far. QDs used in this study are potentially toxic substances because the semiconductor crystal core contains cadmium and selenium. Toxicity of QDs depends on multiple factors, e.g., size, charge, concentration, outer coating bioactivity, and stability of the QD.[29] A recent study reported that mice tolerated intravenous injection of QDs well up to 133 days after administration. Neither signs of necrosis at sites of deposition nor signs of QD breakdown were observed.[30] The QDs used in that study are from the same supplier as the QDs of the current study.

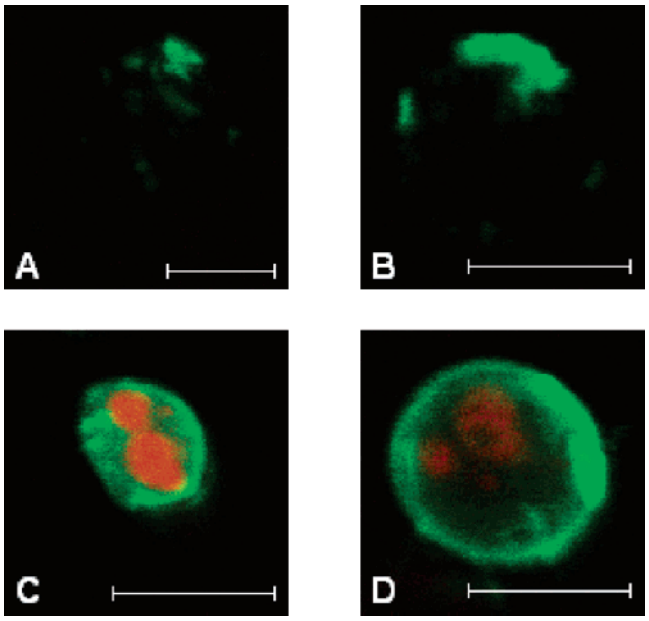

Figure 4. TPLSM images showing cellular AnxA5-QD525 (green) distribution. All cells were counterstained with PI (red) to determine membrane leakage, i.e., determine the stage of apoptosis. Top row: early apoptotic Jurkat cells labeled with (A) AnxA5-QD-Gd and (B) AnxA5-QD-Gd-wedge. Bottom row: late apoptotic cells labeled with (C) AnxA5-QD-Gd and (D) AnxA5-QD-Gd-wedge. Bar = 10 μm.

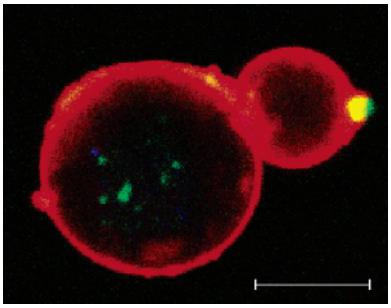

Figure 5. TPLSM image of a Jurkat cell, incubated with AnxA5-QD525-Gd (green), while simultaneously inducing apoptosis by anti-Fas antibodies. After 5.5 h, cells were washed in EDTA buffer to remove AnxA5 present on the outside of the cells and subsequently stained with AnxA5-QD585-Gd (red). Yellow indicates colocalization of QD525 and QD585 (probably caused by QD525 on the cell exterior that had not completely been removed). Cells were counterstained with Syto41 (blue), a nucleic acid stain. Bar = 10 μm.

The present study visualizes QDs by two-photon laser scanning microscopy (TPLSM). The laser power of TPLSM required to have sufficient QD fluorescence is considerably lower as compared to organic fluorescent dyes due to the high quantum yield of QDs. This limits further potential photobleaching of the probe and photodamage of the sample. Furthermore, high-resolution images with low background fluorescence can be acquired. This is due to several factors: First, TPLSM excitation occurs only at the focal point preventing out-of-focus contribution.[31,32] Second, as indicated above, the required laser power is low, thereby also reducing background (auto)fluorescence. Third, because emission spectra of the QDs are narrow,[27] stringent emission filters

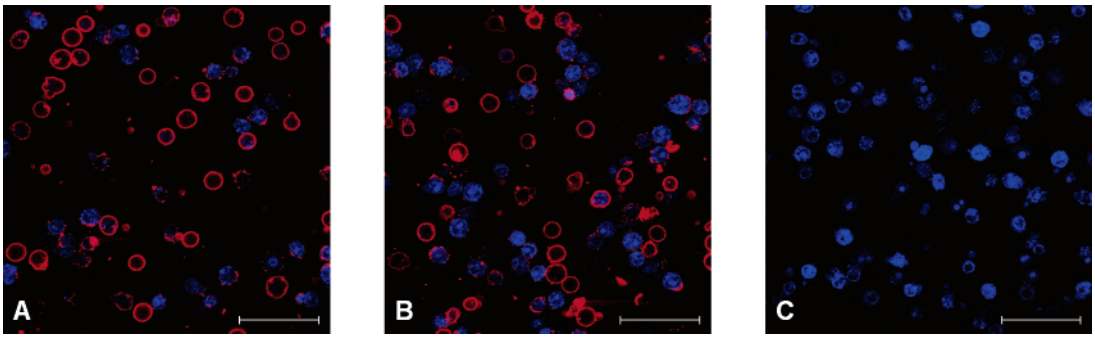

Figure 6. TPLSM images showing the cellular distributions of QD585 (red) coupled to AnxA5 or a mutant of AnxA5, unable to bind to PS (M1234), on apoptotic Jurkat cells. All cells were counterstained with Syto41 (blue), a nucleic acid stain. (A) AnxA5-QD-Gd. (B) AnxA5-QD-Gd-wedge. (C) M1234-QD-Gd-wedge. Bar = 50 μm.

can be applied to reduce background light as much as possible. Hence, it is possible to image structures hidden deeper in tissues more accurately with TPLSM without provoking tissue damage, for example, atherosclerotic plaque imaging in arteries.[31]

The first version of the nanoparticle consisted of biotinylated AnxA5 coupled to streptavidin coated QDs in a 1:1 stoichiometry. QDs had emission peaks of either 525 nm (QD525, green) or 585 nm (QD585, red). AnxA5 contained a single biotin, located apical to the PS binding sites. The remaining binding sites of streptavidin were saturated with biotinylated gadolinium-DTPA,[33] an MRI contrast agent (biotinylated Gd-DTPA, Figure 1A; AnxA5-QD-Gd, Figure 2A).

To increase the perceptibility of the nanoparticle in MRI, it was aimed to increase the load of Gd-DTPA. Therefore, a biotinylated construct was designed consisting of a lysine wedge with eight Gd-DTPA complexes attached to the periphery[34] (Gd-wedge, Figure 1B). Addition of this wedge to the described QDs resulted in the nanoparticle represented in Figure 2B (AnxA5-QD-Gd-wedge). The complete conjugation procedure of the two nanoparticles, along with all other procedures, is available in the Supporting Information.

Low-temperature transmission electron microscopy (cryo-TEM, Figure 3) showed that functionalized QDs in suspension were spherical, monodisperse, and nonaggregated. The spheric diameter was measured to be 6.7 ± 1.0 nm (mean ± standard deviation (SD)), $n = 124$. AnxA5 and Gd-DTPA are not visible on the EM image; however, a gap of at least 1 nm between any two adjacent QDs indicates the presence of molecules on the surface of QDs. These results are similar to results in literature.[35]

In MRI, Gd-DTPA accelerates longitudinal relaxation (T_1 relaxation), which can be quantified by its longitudinal relaxivity (r_1) expressed in mM^{-1} s^{-1}. The r_1 values of AnxA5-QD-Gd and AnxA5-QD-Gd-wedge were estimated based on the r_1 per Gd-DTPA complex, which were subsequently multiplied by the number of Gd-DTPA complexes per nanoparticle. For biotinylated Gd-DTPA coupled to avidin r_1 was 17.5 mM^{-1} s^{-1} per Gd-DTPA,[33] and for biotinylated Gd-wedge coupled to avidin, r_1 was 15.6 mM^{-1} s^{-1} per Gd-DTPA.[34] On the basis of information supplied by the manufacturer (≈ 10 streptavidin molecules per QD), it can be calculated that AnxA5-QD-Gd and AnxA5-QD-Gd-wedge have r_1 values per nanoparticle of 420−630 mM^{-1} s^{-1} and 3000−4500 mM^{-1} s^{-1}, respectively.

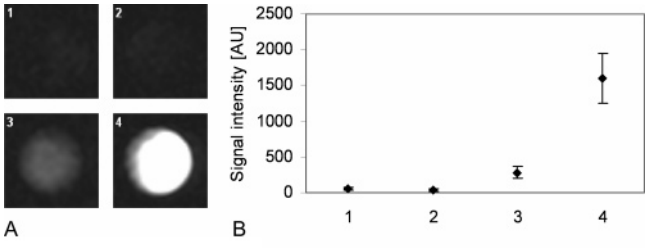

Figure 7. Sections of a single MR image, showing pellets of apoptotic Jurkat cells incubated with AnxA5-QD-Gd or AnxA5-QD-Gd-wedge. (A) T_1-weighted MR-images of the four cell samples. (B) Graph showing mean ±SD for signal intensities of the pixels in the regions of interest (ROIs), drawn within the samples shown in (A). Cells incubated with: **1**, buffer only (control 1); **2**, 1.6 μM Gd-wedge only (control 2); **3**, 40 nM AnxA5-QD-Gd; **4**, 40 nM AnxA5-QD-Gd-wedge.

AnxA5-QD-Gd and AnxA5-QD-Gd-wedge nanoparticles were examined for their property to discriminate between living and dying cells using TPLSM. Jurkat cells were triggered to execute apoptosis by activation of Fas receptor using anti-Fas antibodies. Binding of AnxA5-QD-Gd and AnxA5-QD-Gd-wedge occurred to early and late apoptotic cells but not to viable cells (Figure 4), in a manner comparable to Oregon Green labeled AnxA5 (not shown).[36] During early apoptosis, small patches of green fluorescence were visible on the cellular membrane (Figure 4A,B), whereas during late apoptosis, the entire cellular membrane was brightly fluorescent (Figure 4C,D). The late apoptotic phase is characterized by loss of plasma membrane integrity and concomitant nuclear uptake of propidium iodide (PI), showing a red, fragmented nucleus. In addition, AnxA5-QD-Gd was able to be internalized by Jurkat cells (Figure 5), as was reported for AnxA5.[36] A movie, showing a *z*-stack of a cell, similar to the cell in Figure 5, is also available as Supporting Information. Internalization of AnxA5-QD-Gd-wedge by Jurkat cells was not investigated in this study.

Binding of AnxA5-QD-Gd and AnxA5-QD-Gd-wedge to dying cells depends on cell surface exposure of PS because QDs functionalized with M1234, a variant of AnxA5 that does not bind to PS,[37] do not show binding to apoptotic cells (Figure 6). All together, these findings clearly demonstrate that AnxA5 coupled to a QD retains its full

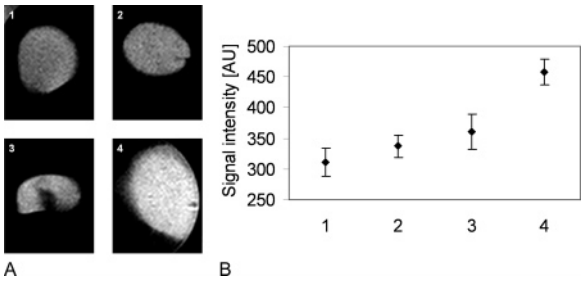

Figure 8. (A) T_1-weighted sections of a single MR image, showing whole-blood clots, activated with Ca^{2+}, thrombin, and collagen, and incubated with AnxA5-QD-Gd-wedge enclosed in 2% agarose gel. (B) graph showing mean ±SD for the signal intensities of the pixels in ROIs, drawn within the samples shown in (A). Clots were incubated with: **1**, buffer only (control 1); **2**, 8 μM Gd-wedge only (control 2); **3**, 40 nM AnxA5-QD-Gd-wedge; **4**, 200 nM AnxA5-QD-Gd-wedge. Clot **3** was slightly damaged, causing the black spot in the clot. Clot **4** was larger probably due to the fact that the higher concentration of AnxA5 inhibited clot retraction through its anticoagulant action.

biological property to bind to PS exposed on the surface of dying cells.

Having established the AnxA5-specific binding properties of AnxA5-QD-Gd and AnxA5-QD-Gd-wedge by fluorescence studies, the functional bimodality of the nanoparticle had to be confirmed. Apoptotic Jurkat cells were incubated with buffer (control 1), Gd-wedge (control 2), AnxA5-QD-Gd, or AnxA5-QD-Gd-wedge and subsequently measured with MRI (Figure 7). The amount of Gd-wedge in sample **2** (control) was equal to the amount used in sample **4**.

Cells incubated with AnxA5-QD-Gd (Figure 7, sample **3**) exhibit a signal intensity that is a factor 5.9 and 6.9 higher as compared to control 1 and control 2, respectively. Cells incubated with AnxA5-QD-Gd-wedge (**4**) exhibit a signal intensity that is a factor 5.8 higher than **3**, demonstrating that AnxA5-QD-Gd-wedge has a much better T_1-lowering effect than AnxA5-QD-Gd, as was expected from the differences in r_1. This results in a higher MRI signal intensity in T_1-weighted imaging using the same amount of nanoparticles.

Cultured cells are simple in vitro systems for testing molecular imaging agents. Results derived from such systems hardly give reliable predictions about behavior in the in vivo situation. Therefore, a more complex system was chosen to assess the robustness of this nanoparticle as a bimodal molecular imaging agent. Because activated platelets expose

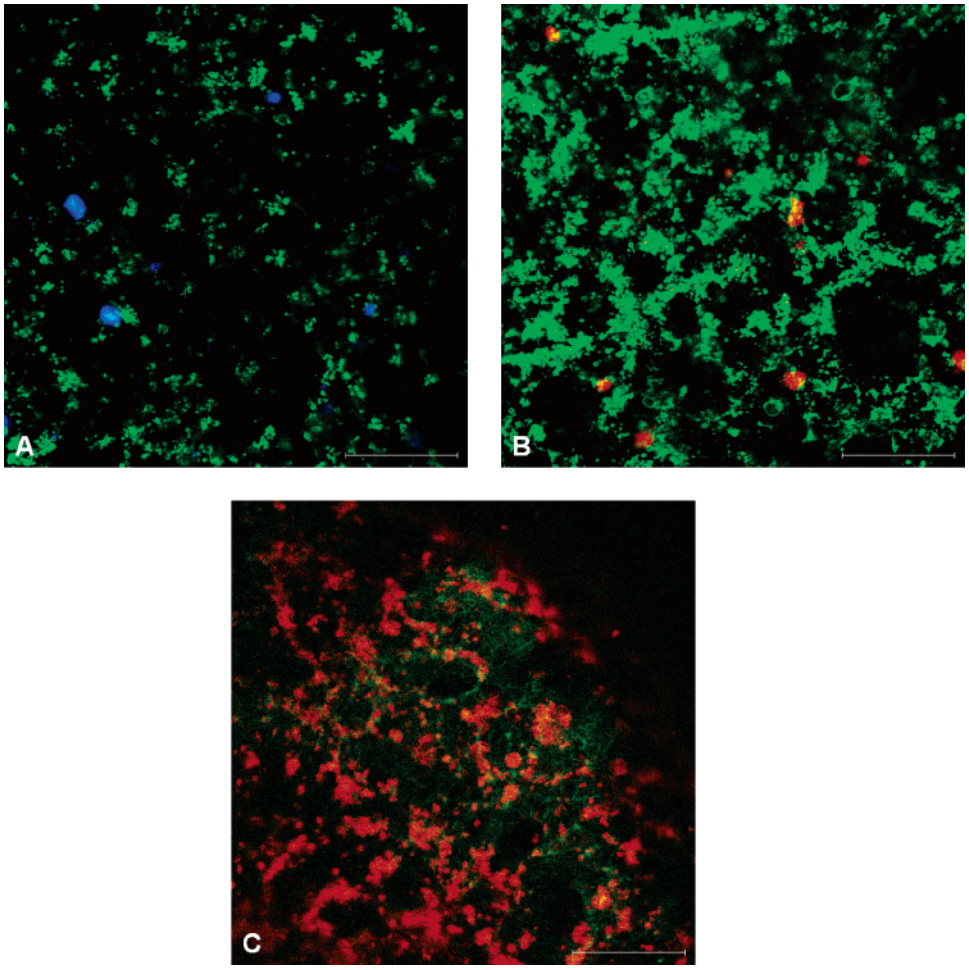

Figure 9. TPLSM images of whole-blood clots incubated with AnxA5 after clot-formation. (A) green: AnxA5-FITC; blue: syto41, a nucleic acid stain; (B) green: AnxA5-QD525-Gd; red: acridine red, a cytoplasmatic stain. (C) red: AnxA5-QD585-Gd; green: anti-fibrinogen-FITC. Platelets show a bright cellular membrane, similar to apoptotic cells (compare to Figures 4,5,6). Bar = 50 μm.

PS, a human whole-blood clot system was chosen. Human whole blood was incubated with AnxA5-QD-Gd-wedge; subsequently, PS exposure by platelets was induced to trigger clot formation. The concentration of nanoparticles within the clot was expected to be much lower as compared to cell pellets. Within the clot, only platelets expose PS, and not, for example, captured erythrocytes. An additional complexity of this system comes from the fact that AnxA5 competes with coagulation factors for binding to PS and acts as an anticoagulant, preventing platelets from being incorporated into the thrombus.[11,38] Hence, MRI signal intensities were not expected to achieve the levels of Figure 7. Therefore, following experiments were performed with AnxA5-QD-Gd-wedge only.

To label as many platelets as possible, whole blood was incubated with AnxA5-QD-Gd-wedge prior to clot formation. Coagulation in whole blood, mediated by thrombin generation and PS exposure on platelets, was triggered by adding Ca^{2+} to citrate-anticoagulated whole blood. Additional PS exposure was triggered by pre-activating the platelets in whole blood with thrombin and collagen[11] to counteract the anticoagulant effect of AnxA5. Whole blood was incubated with buffer (control 1), Gd-wedge (control 2), 40 nM, or 200 nM AnxA5-QD-Gd-wedge; subsequently, clot formation was induced and clots were measured with MRI (Figure 8). The amount of Gd-wedge in sample **2** (control) was equal to the amount used in sample **4**.

Signal intensities of the four clots are shown in Figure 8B. Corresponding T_1 values for clots 1, 2, 3, and 4 are 734 $\pm$ 85, 740 $\pm$ 44, 678 $\pm$ 89, and 628 $\pm$ 30 ms (mean $\pm$ SD), respectively. The signal intensity of clot **4** was approximately 47% and 36% higher than controls **1** and **2**, respectively. These results demonstrate that MRI of PS exposure in a more complex system is feasible using the AnxA5-QD-Gd-wedge nanoparticle. A recent study showed that, with SPECT imaging, mural thrombus renewal in abdominal aortic aneurisms in vivo can be visualized using AnxA5 labeled with a radionuclide.[25] This study proved that thrombus imaging in vivo is feasible using AnxA5.

Whole-blood clots were also analyzed with TPLSM. For TPLSM, clots were incubated with AnxA5-QD-Gd-wedge after clot formation because, in contrast to MRI, a lower amount of AnxA5-QD-Gd-wedge was sufficient for visualization by TPLSM. These experiments could thus be performed without interfering with clot formation.

Distribution of AnxA5-QD-Gd-wedge in the whole-blood clots was similar to the distribution of FITC-labeled AnxA5 (Figure 9A). AnxA5-QD-Gd-wedge specifically labeled activated platelets (Figure 9B,C), as can be deduced from the size of the labeled structures, measuring ca. 1−2 μm. Larger cells incorporated in the clot and easily discernible with a cytoplasm-specific or nucleic acid-specific dye, were stained neither with AnxA5-FITC nor AnxA5-QD-Gd-wedge (Figure 9A,B). Figure 9C shows whole blood that was preincubated with antifibrinogen-FITC and subsequently activated to form a clot. Staining the clot with AnxA5-QD-Gd-wedge reveals that PS exposing platelets are aligned along the fibrin network within the clot.

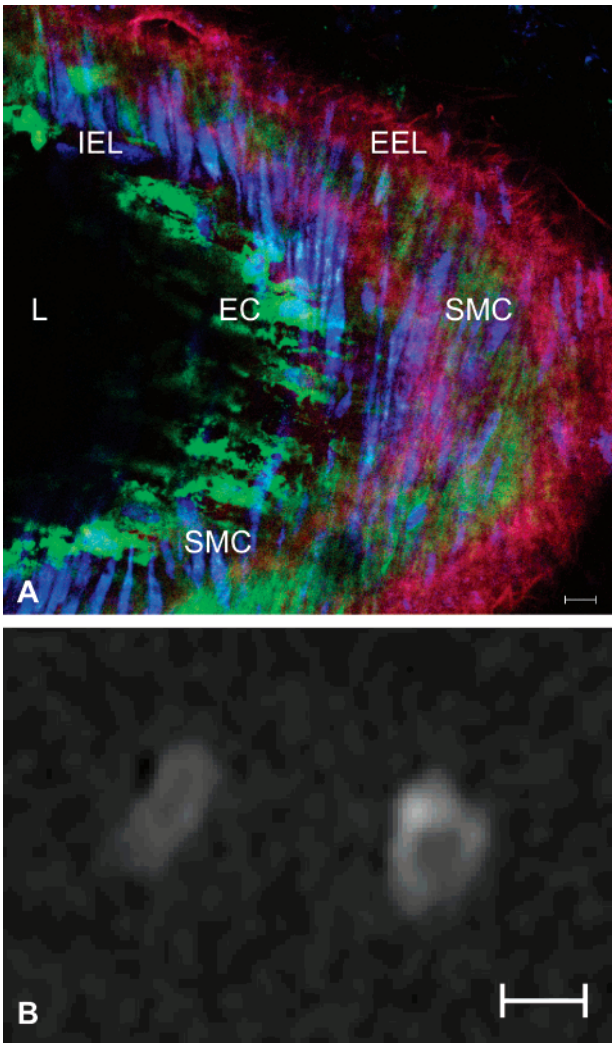

Figure 10. (A) TPLSM image of a wire-injured murine carotid artery, showing the various vascular wall layers. The tunica intima consists of endothelial cells (ECs); the tunica media mainly consists of smooth muscle cells (SMCs). Uptake of nanoparticles is visible in ECs and SMCs. Green: AnxA5-QD-Gd-wedge; red: eosin, labeling elastin laminae; blue: syto41, labeling cell nuclei. L: lumen; IEL: internal elastic lamina; EEL: external elastic lamina. Bar = 10 μm. The imaging plane was slightly oblique, as opposed to a longitudinal direction of the artery. (B) transversal MR image of two murine carotid arteries: undamaged (control, left) and damaged (right, same artery as shown in (A)). Bar = 0.5 mm.

To demonstrate the feasibility of this AnxA5-functionalized bimodal nanoparticle as a target-specific nanoparticle for cell death in the vascular wall, a murine carotid artery was mechanically injured in vivo by endothelial denudation using a metal wire, as described elsewhere.[39] This injury results in rapid PS exposure by cells of the tunica intima, media, and adventitia.[39] Both damaged and undamaged carotid arteries were excised and mounted in a perfusion chamber. A static transmural pressure of 40 mmHg was applied, and the arteries were labeled intraluminally with AnxA5-QD-Gd-wedge by slow perfusion. The arteries were imaged by TPLSM, as described in a recent article.[40] Figure 10A shows uptake of AnxA5-QD-Gd-wedge in the endothelial cells (ECs) in the tunica intima and in smooth muscle cells (SMCs) in the tunica media. Apparently, nanoparticles

Table 1. Comparison of Five Different Bimodal AnxA5-Conjugated Nanoparticles. NIRF = Near-Infrared Fluorescence.

nanoparticle	T_1 or T_2 lowering	size (nm)	r_1	r_2	stoichiometry AnxA5:particle	optical
AnxA5-QD-Gd-wedge[a]	T_1	~7	3000−4500 (mM^{-1} particle) s^{-1}	5600−8400 (mM^{-1} particle) s^{-1}	1:1	visible, NIRF
micellar QD-AnxA5[b]	T_1	<10	~1860 (mM^{-1} particle) s^{-1}	~2700 (mM^{-1} particle) s^{-1}	>5:1[e]	visible, NIRF
AnxA5-fluorescein liposomes[c]	T_1	100	~164 000 (mM^{-1} particle) s^{-1}	~272 000 (mM^{-1} particle) s^{-1}	>5:1[e]	visible
AnxA5-CLIO-Cy5.5[d]	T_2	50	19 (mM^{-1} Fe) s^{-1}	48 (mM^{-1} Fe) s^{-1}	3.5:1	NIRF
AnxA5-fluorescein micellar iron oxide[c]	T_2	10	13.3 (mM^{-1} Fe) s^{-1}	159.6 (mM^{-1} Fe) s^{-1}	>5:1[e]	visible

[a] This paper. [b] van Tilborg et al. [43] [c] van Tilborg et al. [20] [d] Schellenberger et al.[19] [e] Personal communication.

are able to penetrate through elastic laminae deep into the tunica media. It is unclear why the first SMC layer hardly shows any uptake of the nanoparticle, while the layer of SMCs between the outer two elastic laminae does show abundant labeling. Furthermore, no labeled platelets were visible, as no blood was present at time of labeling. A movie of a three-dimensional representation of the carotid artery in Figure 10A is available as Supporting Information. The undamaged control artery hardly shows any labeling. Next, the arteries were removed from the perfusion chamber and embedded in agarose gel for imaging with MRI. The amount of labeling of the damaged artery is sufficient to increase the MRI signal intensity compared to the control artery (Figure 10B). To determine the increase in signal intensity, three transversal MRI slices of the carotid arteries were divided into quadrants. In these quadrants, ROIs were drawn to select the vascular wall. This is because the uptake of nanoparticle was not homogeneous throughout the vascular wall, as it was unevenly damaged by the wire. A total of twelve signal intensities was acquired per artery. The mean signal intensity increased from 83.2 ± 3.6 for the control artery to 91.9 ± 13.5 for the damaged artery (arbitrary units, mean ± SD) and ranging from 73.5 to 86.9 for the control artery and 73.4 to 125 for the damaged artery. This indicates that the increase in signal intensity differs per location in the vascular wall and ranges from 0 to 50% compared to the control, undamaged artery.

Reports about QD-labeled AnxA5 have been published recently. As mentioned before, Le Gac et al.[28] investigated photostability of streptavidin-coated, AnxA5-labeled QDs. In contrast to the biotinylated AnxA5 used in this study, the described AnxA5 contained three to four biotins, located at random sites on the AnxA5 polypeptide. This implies, as pointed out by the authors, that AnxA5 coupling to QDs may lead to masking of PS binding sites and aggregation of the QDs. The current study utilized cys2-AnxA5, which contains a single biotin attached to the *N*-terminal tail that is located opposite to the side of the AnxA5 molecule harboring the PS binding sites.[41] Coupling of cys2-AnxA5 to streptavidin-coated QDs neither induced aggregation nor caused a loss of biological activity. In addition, a recent study[42] showed that cells, labeled with AnxA5-QDs, can be imaged using an in vivo imaging system.

Another study investigated bimodal, paramagnetic micellular QDs that were functionalized with AnxA5.[43] Table 1 summarizes the most important characteristics of AnxA5-functionalized bimodal nanoparticles published in literature. Two other T_1-weighted nanoparticles, loaded with Gd-DTPA, are compared with the novel nanoparticle described in the current study. Furthermore, two T_2-weighted nanoparticles, containing iron oxide, are listed. AnxA5-QD-Gd-wedge has several advantages. First, it is the smallest nanoparticle so far. This can be advantageous when the imaging target is outside the vessel lumen, as in, for example, atherosclerotic plaques or tumors. Furthermore, of the T_1-weighted nanoparticles, AnxA5-QD-Gd-wedge is the nanoparticle with the highest relaxivity relative to the nanoparticle surface area. AnxA5-QD-Gd-wedge allows visible and near-infrared imaging and shows high fluorescence intensities. Additionally, QDs can be localized by electron microscopy.[35] Moreover, the 1:1 stoichiometry of the AnxA5-QD complex provides the most optimal configuration for maximizing the amount of bimodal nanoparticle bound to the PS exposing surface. Other advantages of AnxA5-QD-Gd-wedge are straightforward preparation (add and mix) and variability of the nanoparticle's biological functionality. By replacing AnxA5 by a different biotinylated targeting function, this nanoparticle can be used for molecular imaging of different biological processes.[44]

The results in this paper demonstrate that the bimodal AnxA5-QD-Gd-wedge nanoparticle can be used to analyze biological samples as well as vascular structures with MRI at the anatomical level and with TPLSM at the cellular level. AnxA5-QD-Gd-wedge has high potential for in vivo imaging in the near future.

Acknowledgment. We thank Dr. Wim Engels for his assistance with the TPLSM experiments, and Dr. Walter Backes for performing the preliminary MRI experiments. This work was financed by SenterNovem, BSIK 03033; TPLSM was financed by The Netherlands Organization for Scientific Research, NWO 902-16-276.

Supporting Information Available: All experimental procedures are described. Also, two movies are available, one showing a *z*-stack of an apoptotic Jurkat cell with

internalized AnxA5-QD-Gd and one showing a three-dimensional view of the carotid artery in Figure 10A. This material is available free of charge via the Internet at http://pubs.acs.org.

References

(1) Kroemer, G.; El-Deiry, W. S.; Golstein, P.; Peter, M. E.; Vaux, D.; Vandenabeele, P.; Zhivotovsky, B.; Blagosklonny, M. V.; Malorni, W.; Knight, R. A.; Piacentini, M.; Nagata, S.; Melino, G. *Cell Death Differ.* **2005**, *12* (Suppl 2), 1463−1467.

(2) Hofstra, L.; Liem, I. H.; Dumont, E. A.; Boersma, H. H.; van Heerde, W. L.; Doevendans, P. A.; De Muinck, E.; Wellens, H. J.; Kemerink, G. J.; Reutelingsperger, C. P.; Heidendal, G. A. *Lancet* **2000**, *356*, 209−212.

(3) Narula, J.; Haider, N.; Virmani, R.; DiSalvo, T. G.; Kolodgie, F. D.; Hajjar, R. J.; Schmidt, U.; Semigran, M. J.; Dec, G. W.; Khaw, B. A. *N. Engl. J. Med.* **1996**, *335*, 1182−1189.

(4) Isner, J. M.; Kearney, M.; Bortman, S.; Passeri, J. *Circulation* **1995**, *91*, 2703−2711.

(5) Geng, Y. J.; Libby, P. *Am. J. Pathol.* **1995**, *147*, 251−266.

(6) Evan, G. I.; Vousden, K. H. *Nature* **2001**, *411*, 342−348.

(7) Hu, W.; Kavanagh, J. J. *Lancet Oncol.* **2003**, *4*, 721−729.

(8) Corsten, M. F.; Hofstra, L.; Narula, J.; Reutelingsperger, C. P. *Cancer Res.* **2006**, *66*, 1255−1260.

(9) Haas, R. L.; de Jong, D.; Valdes Olmos, R. A.; Hoefnagel, C. A.; van den Heuvel, I.; Zerp, S. F.; Bartelink, H.; Verheij, M. *Int. J. Radiat. Oncol., Biol., Phys.* **2004**, *59*, 782−787.

(10) Savill, J.; Fadok, V. *Nature* **2000**, *407*, 784−788.

(11) Thiagarajan, P.; Tait, J. F. *J. Biol. Chem.* **1990**, *265*, 17420−17423.

(12) Munnix, I. C.; Strehl, A.; Kuijpers, M. J.; Auger, J. M.; van der Meijden, P. E.; van Zandvoort, M. A.; oude Egbrink, M. G.; Nieswandt, B.; Heemskerk, J. W. *Arterioscler., Thromb., Vasc. Biol.* **2005**, *25*, 2673−2678.

(13) Boersma, H. H.; Kietselaer, B. L.; Stolk, L. M.; Bennaghmouch, A.; Hofstra, L.; Narula, J.; Heidendal, G. A.; Reutelingsperger, C. P. *J. Nucl. Med.* **2005**, *46*, 2035−2050.

(14) Reutelingsperger, C. P.; van Heerde, W. L. *Cell. Mol. Life Sci.* **1997**, *53*, 527−532.

(15) van Engeland, M.; Nieland, L. J.; Ramaekers, F. C.; Schutte, B.; Reutelingsperger, C. P. *Cytometry* **1998**, *31*, 1−9.

(16) van den Eijnde, S. M.; Luijsterburg, A. J.; Boshart, L.; De Zeeuw, C. I.; van Dierendonck, J. H.; Reutelingsperger, C. P.; Vermeij-Keers, C. *Cytometry* **1997**, *29*, 313−320.

(17) Reutelingsperger, C. P.; Dumont, E.; Thimister, P. W.; van Genderen, H.; Kenis, H.; van de Eijnde, S.; Heidendal, G.; Hofstra, L. *J. Immunol. Methods* **2002**, *265*, 123−132.

(18) Toretsky, J.; Levenson, A.; Weinberg, I. N.; Tait, J. F.; Uren, A.; Mease, R. C. *Nucl. Med. Biol.* **2004**, *31*, 747−752.

(19) Schellenberger, E. A.; Sosnovik, D.; Weissleder, R.; Josephson, L. *Bioconjugate Chem.* **2004**, *15*, 1062−1067.

(20) van Tilborg, G. A.; Mulder, W. J.; Deckers, N.; Storm, G.; Reutelingsperger, C. P.; Strijkers, G. J.; Nicolay, K. *Bioconjugate Chem.* **2006**, *17*, 741−749.

(21) Johnson, L. L.; Schofield, L.; Donahay, T.; Narula, N.; Narula, J. *J. Nucl. Med.* **2005**, *46*, 1186−1193.

(22) Kietselaer, B. L.; Reutelingsperger, C. P.; Heidendal, G. A.; Daemen, M. J.; Mess, W. H.; Hofstra, L.; Narula, J. *N. Engl. J. Med.* **2004**, *350*, 1472−1473.

(23) Keen, H. G.; Dekker, B. A.; Disley, L.; Hastings, D.; Lyons, S.; Reader, A. J.; Ottewell, P.; Watson, A.; Zweit, J. *Nucl. Med. Biol.* **2005**, *32*, 395−402.

(24) Blankenberg, F. G.; Katsikis, P. D.; Tait, J. F.; Davis, R. E.; Naumovski, L.; Ohtsuki, K.; Kopiwoda, S.; Abrams, M. J.; Darkes, M.; Robbins, R. C.; Maecker, H. T.; Strauss, H. W. *Proc. Natl. Acad. Sci. U.S.A.* **1998**, *95*, 6349−6354.

(25) Sarda-Mantel, L.; Coutard, M.; Rouzet, F.; Raguin, O.; Vrigneaud, J. M.; Hervatin, F.; Martet, G.; Touat, Z.; Merlet, P.; Le Guludec, D.; Michel, J. B. *Arterioscler., Thromb., Vasc. Biol.* **2006**, *26*, 2153−2159.

(26) Miserus, R. J. J. H. M.; Heeneman, S.; Engelshoven, J. M. A. v.; Kooi, M. E.; Daemen, M. J. A. P. *Drug Disc. Today: Technol.* **2006**, *3*, 195−204.

(27) Watson, A.; Wu, X.; Bruchez, M. *BioTechniques* **2003**, *34*, 296−300, 302−303.

(28) Le Gac, S.; Vermes, I.; van den Berg, A. *Nano Lett.* **2006**, *6*, 1863−1869.

(29) Hardman, R. *Environ. Health Perspect.* **2006**, *114*, 165−172.

(30) Ballou, B.; Lagerholm, B. C.; Ernst, L. A.; Bruchez, M. P.; Waggoner, A. S. *Bioconjugate Chem.* **2004**, *15*, 79−86.

(31) van Zandvoort, M.; Engels, W.; Douma, K.; Beckers, L.; Oude Egbrink, M.; Daemen, M.; Slaaf, D. W. *J. Vasc. Res.* **2004**, *41*, 54−63.

(32) Denk, W.; Strickler, J. H.; Webb, W. W. *Science* **1990**, *248*, 73−76.

(33) Langereis, S.; Kooistra, H. A.; van Genderen, M. H.; Meijer, E. W. *Org. Biomol. Chem.* **2004**, *2*, 1271−1273.

(34) Dirksen, A.; Meijer, E. W.; Adriaens, W.; Hackeng, T. M. *Chem. Commun.* **2006**, 1667−1669. A manuscript on the synthesis and characterization of Gd-wedge is in preparation.

(35) Giepmans, B. N.; Deerinck, T. J.; Smarr, B. L.; Jones, Y. Z.; Ellisman, M. H. *Nat. Methods* **2005**, *2*, 743−749.

(36) Kenis, H.; van Genderen, H.; Bennaghmouch, A.; Rinia, H. A.; Frederik, P.; Narula, J.; Hofstra, L.; Reutelingsperger, C. P. *J. Biol. Chem.* **2004**, *279*, 52623−52629.

(37) Mira, J. P.; Dubois, T.; Oudinet, J. P.; Lukowski, S.; Russo-Marie, F.; Geny, B. *J. Biol. Chem.* **1997**, *272*, 10474−10482.

(38) Ramstrom, S.; Ranby, M.; Lindahl, T. L. *Thromb. Haemostasis* **2003**, *89*, 132−141.

(39) Ravassa, S.; Bennaghmouch, A.; Kenis, H.; Lindhout, T.; Hackeng, T.; Narula, J.; Hofstra, L.; Reutelingsperger, C. *J. Biol. Chem.* **2005**, *280*, 6028−6035.

(40) Megens, R. T. A.; Reitsma, S.; Schiffers, P. H. M.; Hilgers, R. H. P.; De Mey, J. G. R.; Slaaf, D. W.; oude Egbrink, M. G. A.; van Zandvoort, M. A. M. J. *J. Vasc. Res.* **2006**, in press.

(41) Huber, R.; Schneider, M.; Mayr, I.; Romisch, J.; Paques, E. P. *FEBS Lett.* **1990**, *275*, 15−21.

(42) Dicker, D. T.; Kim, S. H.; Jin, Z.; El-Deiry, W. S. *Cancer Biol. Ther.* **2005**, *4*, 1014−1017.

(43) van Tilborg, G. A.; Mulder, W. J.; Chin, P. T.; Storm, G.; Reutelingsperger, C. P.; Nicolay, K.; Strijkers, G. J. *Bioconjugate Chem.* **2006**, *17*, 865−868.

(44) Buehler, A.; van Zandvoort, M. A. M. J.; Stelt, B. J.; Hackeng, T. M.; Schrans-Stassen, B. H. G. J.; Bennaghmouch, A.; Hofstra, L.; Cleutjens, J. P. M.; Duijvestijn, A.; Smeets, M. B.; de Kleijn, D. P. V.; Post, M. J.; de Muinck, E. D. *Arterioscler., Thromb., Vasc. Biol.* **2006**, *26*, 2681−2687.

NL062226R